NANO LETTERS

2007
Vol. 7, No. 3
632−637

Deformation-Driven Electrical Transport of Individual Boron Nitride Nanotubes

Xuedong Bai,[†] Dmitri Golberg,*[,‡] Yoshio Bando,[†,‡] Chunyi Zhi,[‡] Chengchun Tang,[‡] Masanori Mitome,[‡] and Keiji Kurashima[‡]

International Center for Young Scientists, and Nanoscale Materials Center, National Institute for Materials Science, Namiki 1-1, Tsukuba, Ibaraki 305-0044, Japan

Received October 29, 2006; Revised Manuscript Received January 24, 2007

ABSTRACT

In contrast to standard metallic or semiconducting graphitic carbon nanotubes, for years their structural analogs, boron nitride nanotubes, in which alternating boron and nitrogen atoms substitute for carbon atoms in a graphitic network, have been considered to be truly electrically insulating due to a wide band gap of layered BN. Alternatively, here, we show that under in situ elastic bending deformation at room temperature inside a 300 kV high-resolution transmission electron microscope, a normally electrically insulating multiwalled BN nanotube may surprisingly transform to a semiconductor. The semiconducting parameters of bent multiwalled BN nanotubes squeezed between two approaching gold contacts inside the pole piece of the microscope have been retrieved based on the experimentally recorded *I*–*V* curves. In addition, the first experimental signs suggestive of piezoelectric behavior in deformed BN nanotubes have been observed.

Boron nitride nanotubes (BNNTs), which represent an important class of inorganic nanotubes, have attracted significant attention since their theoretical prediction in 1994.[1] Structurally, BNNT is similar to a carbon nanotube (CNT). However, electronically, BNNT is quite different from its carbon counterpart. Because of its ionic origin the BNNT band gap (∼5.5 eV) is almost independent of tube diameter, number of shells, and chirality.[2] Therefore, normally, BNNTs are insulating.[3] On the other hand, a recent theoretical work on BNNTs under flattening deformation[4] has predicted the unique possibility of band gap tuning in a 2−5 eV range, i.e., electrical response may vary from insulating to semiconducting. BNNTs have excellent mechanical properties; their elastic modulus is nearly analogous to that of CNTs [5] as measured and/or calculated on multiwalled BNNTs.[6−8] BNNTs were also predicted to exhibit a piezoelectricity.[9−11] Thus these NTs have a high potential for applications in nanometer scale sensors, actuators, and advanced nanoelectromechanical systems (NEMS) with integrated electronic/optoelectronic functions. Here, we show the striking effects of mechanical deformation on an electrical response of multiwalled BNNTs under nanomanipulation and nanoprobing in a 300 kV high-resolution analytical transmission electron microscope. The bending deformation results in the dramatic BNNT electrical transition from an insulator to a semiconductor. The semiconductor parameters of deformed BNNTs, including resistivity, carrier concentration, and their mobility, were extracted from the experimental *I*−*V* curves. It is worth noting that the deformation-induced electrical effects in BNNTs, which include an unusual piezoelectric-like behavior, have been predicted theoretically but never observed experimentally; thus the regarded work provides the first experimental observation of these unique phenomena.

The experiments were carried out by using a Nanofactory Instruments scanning tunneling microscope (STM)−transmission electron microscope (TEM) joint instrument[12] inserted into a JEM-3100FEF (JEOL) 300 kV field-emission high-resolution TEM. An STM probe attached to a piezomotor was controlled by the commercial software and electronics from Nanofactory Instruments AB.[13] A sharp metallic STM tip was fixed on the moveable end of a piezotube, facing its opposite electrode, i.e., another metal tip, and oriented perpendicular to an electron beam of TEM. An STM and a counter tip/electrode were made of gold, platinum, or tungsten in multiple experimental runs. A nanotube sample was first attached onto either an STM tip or its opposite counter tip/electrode. Then it was tightly fixed on the tip through manual manipulation with tweezers, and the position of the counter electrode was adjusted to obtain the minimal possible gap distinguished by eye between the metallic contacts in an optical microscope. The electron microscope was equipped with an electron energy loss spectrometer (EELS, Omega filter) and an energy dispersion X-ray detector (EDS, Noran). Therefore, the precise structural and chemical analysis before, under, and after manipulation/

* Corresponding author. E-mail: GOLBERG.dmitri@nims.go.jp.
[†] International Center for Young Scientists.
[‡] Nanoscale Materials Center.

10.1021/nl062540l CCC: $37.00
Published on Web 02/09/2007

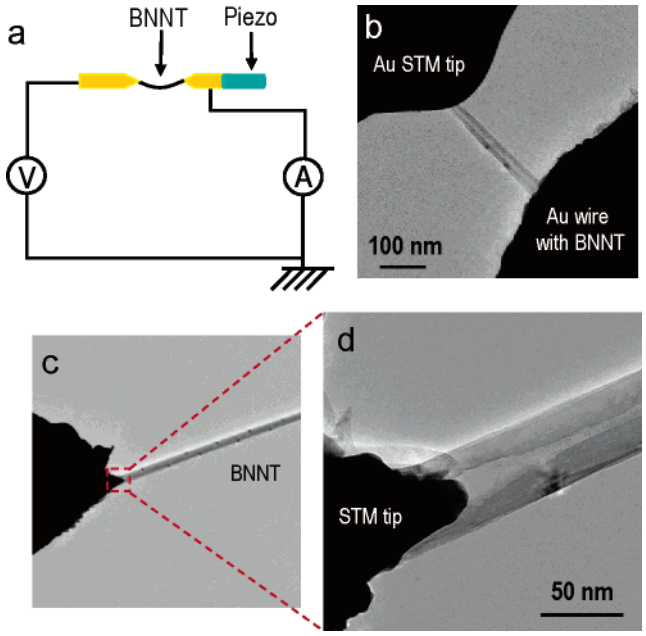

Figure 1. (a) Schematic drawing of the experimental setup. (b) STM tip contacting a BN nanotube inside TEM. (c) Image of a STM tip contacting a multiwalled BN nanotube at the improved physical contact between the tip and the tube. (d) Enlarged TEM image of the contact area in (c) with the tip penetrated inside the tube.

deformation/electrical probing can be performed in situ through parallel TEM imaging, electron diffraction, and spatially resolved spectroscopic methods. The BNNTs were prepared via a carbon-free chemical vapor deposition method.[14] A mixture of MgO and FeO or SnO and a boron powder was used to produce the catalyst and boron oxide vapors. The vapor-phase reactions between a boron oxide and a supplying ammonia gas at a high temperature produced the bulk quantities of impurity-free multiwalled BNNTs.

Figure 1a shows a simplified scheme utilized for the electrical measurements and manipulation using the TEM−STM instrument. A piezodriven stage with an etched STM tip served as a moveable electrode, and another sharply etched metal tip served as its counterpart. The BNNT sample is attached onto either tip using a sticky graphite paste. The STM tip positions could be easily controlled in three dimensions, *X*, *Y*, and *Z*, within the pole piece of the microscope in a wide spatial range to make a decent on-demand contact and/or to manipulate with an individual BNNT. Figure 1b displays an STM tip contacting a BNNT. The sample status could be checked in a real time inside the microscope, while all conventional TEM operations, e.g., lattice-resolved imaging, electron diffraction, spatially resolved EELS, and EDX are also readily available. The two-terminal $I-V$ curves were measured using a "Nanofactory Instruments" (a maximum voltage ±140 V) power generator.[15]

First, we emphasize here that it is crucial to make a good physical contact between an electrode and a BNNT during electrical probing. In this study, when a STM probe mechanically contacted a nanotube, a moderate current of several dozens of nA was applied to pass through the

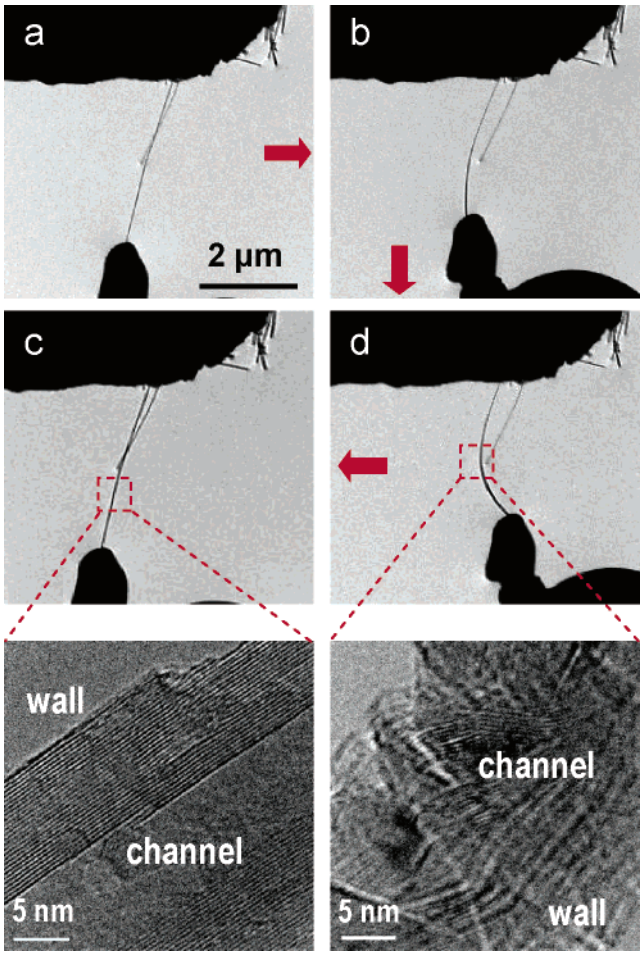

Figure 2. (a−d) Sequential images of a given BNNT bending and relief process inside TEM; bottom insets show the HRTEM images of the relaxed and heavily elastically bent BNNT matching the framed areas in (c) and (d), respectively.

electrode−nanotube circuit. Because of a high resistance of the contact points, a locally high temperature can be generated. This caused the metal probe nanowelding to a nanotube and forming a perfect physical contact between the two. Figure 1c shows the most effective method to improve the intimacy of a physical contact. If a STM tip is sharp enough (a radius of curvature of ∼several nanometers), it may be inserted into the hollow channel of a nanotube. Then, a moderate current was again applied to weld the nanotube to the electrode. Figure 1d is the enlarged TEM images of the contact area with the tip penetrated into the tube. In contrast to the previously reported standard two-terminal or four-terminal electrical measurements of nanotubes in which only the outer wall of a multiwalled nanotube was in contact with the electrical leads (thus only its outermost wall participated in the electrical transport), the technique developed here allows all tubular shells to simultaneously participate in the transport.

Figure 2a−d displays the sequential images of a representative BNNT during a gradual increase in its bending curvature σ under the gentle moves of a piezodriven electrode. In this particular case, both electrodes were made of gold. Importantly, the deformation can be fully recovered using the delicate STM manipulation. Surprisingly, the

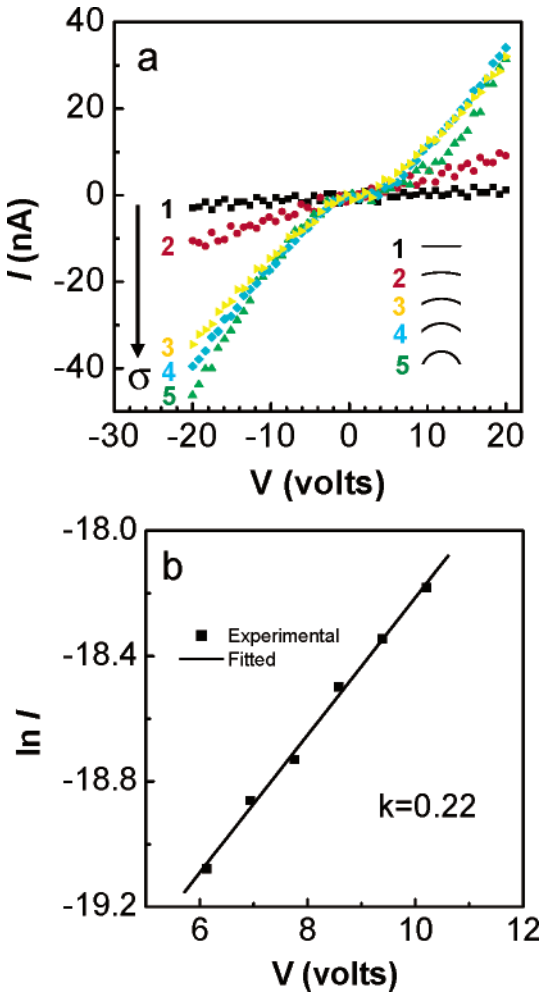

Figure 3. (a) Serials of the representative $I-V$ curves along with an increase in a BNNT bending curvature, σ; an approximate NT curvature is depicted on the right-hand legend. (b) Experimental and fitted ln$I$ vs V plots at intermediate bias using the $I-V$ curve 4 in (a).

BNNTs revealed a remarkably high elasticity, which has been hardly a priori expected for a somewhat ioniclike BN layered compound. In the present experiments, the BNNTs, bent over their elastic limit, usually broke, so no plastic deformation was observed. The multiwalled BNNTs were found to be markedly flattened, while bent, as shown in the high-resolution TEM image corresponding to the framed area in Figure 2d. The graphitic lattice was recovered when the nanotube was relaxed, as shown in the high-resolution TEM image corresponding to the framed area in Figure 2c. It is noted that, in the bending area, the rippled distortion can be seen.[16] It is a bit different from the smooth profile of the rippled CNT,[17] which may be caused by the relative brittleness of BNNTs compared to CNTs.

Figure 3a presents a series of consecutively recorded $I-V$ curves along with an increase in BNNT bending curvature. For an initial two-end clamped not-bent BNNT, a meaningful current could be hardly detected (black squares). When the BNNT was slightly bent through delicate driving of the STM tip, a passing current of several nA at a voltage of several V (red circles) was recorded. However, the nanotube resistance R still remains high, ~2 GΩ. The high-resistant $I-V$ curve is basically linear, which still demonstrates the characteristics of an insulator. With increasing in a tube bending curvature, the current remarkably increases starting from a ±5 V bias (yellow side triangles). In a large bias regime, the $I-V$ curve can be differentiated to obtain a resistance R of the nanotube, $R \sim dV/dI$. For this bending curvature, the resistance R largely decreases, up to ~480 MΩ. The R continues to decrease to ~260 MΩ (green upper triangles) with a further increase in a bending curvature. Interestingly enough, during the experiments, when a BNNT bending state was nearly recovered to its initial state, the $I-V$ characteristics were also recovered. Starting from a moderate bending curvature, the $I-V$ curve basically demonstrates the symmetry and current values suggestive of a semiconductor. Thus, the measured system as a whole can be regarded as a metal−semiconductor−metal circuit. The carrier type of the BNNTs was first checked through fabricating a BNNT field-effect transistor (see Supporting Information and Figure S1). Because the work function of gold (~5.1 eV) is less than that of BNNT, and the BNNTs behave as p-type semiconductors, the two contacts could be considered to be of Schottky type. Therefore, the observed $I-V$ characteristics should be modeled by treating the transport in the BNNT as in a metal−semiconductor−metal circuit involving the two Schottky barriers and a resistor in between. For two such Schottky barriers, if one is forwardly biased, the other becomes reversely biased, and vice versa. Because a tunneling current becomes the dominating mechanism under reverse bias in low-dimensional systems,[18] the electrical transport can be dominated by the reverse-biased Schottky barrier under an intermediate bias.

To evaluate the possible influence of the contact material on the observed deformation-driven electrical phenomena and exclude possible artifacts, we carried out the analogous test experiments by changing both gold contacts to platinum contacts (Pt work function $\phi \sim 6.1$ eV, $>\phi$ of BNNT) and by changing one gold tip to a tungsten tip (W work function $\phi \sim 4.5$ eV, $<\phi$ of BNNT). The regarded electrical phenomena were again observed under deformation (see Supporting Information and Figure S2). Therefore, we emphasize here that the observed electrical transition is not related to a metal contact type. On the other hand, in the case of BNNTs, in contrast to CNTs, no matter what kind of a metal electrode is used and how good the physical contact is, any current is hardly passed through a tube in its nondeformed state, up to a very high applied bias voltage. In addition, other test experiments, in which two metal contacts approach each other (without a BNNT sample mounted) were performed to evaluate a field-emission current appearing between the metal electrodes under biasing. At the same distances between the metal leads and same bias voltages that were used in the above-mentioned experiments with the BNNTs, a current can hardly reach several nA, that is, much lower than in a nanotube-containing circuit. Therefore, the mechanical deformation is an essential mean for the observed transition of the BNNT electrical performance, albeit the contact indeed may play an important role for the semiconducting transport in the BNNT system.

Table 1. Electrical Parameters of a Bent BNNT under Increasing of Its Bending Curvature

bending curvature σ	1	2	3	4	5
resistance (GΩ)	12	2	0.48	0.42	0.26
resistivity (Ω cm)	-	-	22.6	19.3	12.2
hole concentration (/cm3)	-	-	1.1×10^{17}	1.6×10^{17}	2.8×10^{17}
mobility (cm^2/V s)	-	-	2.50	2.02	1.83

We also analyzed the structure of BNNTs during in situ TEM while probing. Among all BNNTs studied, there was a notable tendency for the so-called "zigzag" atomic arrangement of the tubular graphitic sheets with respect to the tube axes (see Supporting Information and Figure S3). It is noted, though, that the striking change in the electronic behavior was also found in the case of other monochiral and multichiral BNNTs. So far, the role of nanotube chirality is not yet clear. During structural characterization and sample manipulation inside TEM, we tried to minimize the electron beam effects by choosing a very low beam current density (at least half of that used under normal imaging conditions of 1−2 A/cm^2). In addition, we shut off the electron beam when the $I-V$ curves were recorded. Thus, the related contamination and electron-beam-induced structural damage were fully excluded or, at least, decently minimized. For the sake of clarity and control, after several cycles of bending and consecutive $I-V$ curve recording, the EELS spectra were taken from the tested BNNT. These show pure BNNT compositions with atomic ratios of B/N close to 1.0. No other signals (related to the tube contaminations) were detected (see Supporting Information and Figure S3).

The semiconductor parameters can be retrieved from the $I-V$ curves[19,20] in the intermediate bias regime where the reverse-biased Schottky barrier dominates the total current I:

$$\ln I = \ln(SJ) + V\left(\frac{q}{kT} - \frac{1}{E_0}\right) + \ln J_S \qquad (1)$$

where J is the current density through a Schottky barrier, J_S is a slowly varying function of an applied bias, and S is the contact area associated with a barrier; in turn, E_0 is given by the equation: $E_0 = E_{00} \coth(E_{00}/kT)$, where $E_{00} = \hbar q/2(n/m^*\epsilon)^{1/2}$, n is hole concentration, m^* is an effective hole mass of a bent BNNT, and ϵ is the dielectric constant. The logarithmic plot of a current I as a function of a bias V gives an approximately straight line with a slope of $q/(kT) - 1/E_0$, as depicted in Figure 3b.

Thus, the hole concentration n can be acquired via E_0, and a carrier mobility μ can be obtained from the resistivity ρ of a bent nanotube. Applying this procedure to the $I-V$ curves in Figure 3a, the bent BNNT resistance, resistivity, hole concentration, and carrier mobility were extracted, as summarized in Table 1.

It is well-known that a free-standing nondeformed BNNT is electrically insulating. Needless to say, it is quite puzzling that the electronic structure of BNNTs can be tuned from insulating to semiconducting through a bending deformation. Theoretically, the band gap of a single-walled BNNT could be changed within a large range (2−5 eV) by cross-section flattening.[4] In this study, the multiwalled BNNTs were found to be markedly flattened, while bent, as shown in the high-resolution TEM image of Figure 2. In fact, the nanotube became largely flattened, and a spacing between the two opposite sides of the inner wall becomes very close to an interlayer basal plane spacing in the standard layered (hexagonal or rhombohedral) BN system (∼0.333 nm). Also, an improved physical contact between the electrodes and nanotubes makes all walls of a BNNT simultaneously participate in the electrical transport, that is to say, the detected current is from the all parallel-connected shells, and each shell is equivalent to a single-walled nanotube. Therefore, the experimental results can be analyzed in the light of these specific characteristics.

Another possible reason that accounts for the experimentally observed deformation-driven transport may be bending-induced in-shell defect formation (e.g., voids, vacancies, antisite atoms, etc.), which should also modify the band structure. The defects may appear on bending[21] but disappear after a load release. In our recent work, we demonstrated that heavily corrupted elastically deformed BNNT layers may fully restore their original shape and structural perfection upon unloading.[16]

The local electronic structure can be in situ probed using EELS. The evolutions of the EELS spectra under bending were recorded (see Supporting Information and Figure S4). With increasing a bending curvature, the consecutive changes in the boron K edge fine structure become visible. The fine structure of a σ^* peak and the intensity ratio of π^* and σ^* peaks are obviously changed. This is direct evidence of the highly localized modifications of the electronic structure induced by BNNT bending.

The bending effect on the electrical transport was typically more obvious for the shorter BNNTs. For the longer BNNTs, only negligible flattening deformation may occur near the contact points such that the overall bending effect becomes weak.

In the course of this work, it was additionally found that the electrical performance of deformed BNNTs is suggestive of the piezoelectric effects. For example, an $I-V$ curve was first recorded through voltage sweeping from a negative to a positive range. During the second sweeping, a voltage was applied in the reverse direction, from the positive to negative values. It is notable that a distinct $I-V$ hysteresis appears. Figure 4a shows a representative $I-V$ hysteresis loop recorded on a deformed BNNT.

We then use a simple model to analyze this interesting electrical phenomenon regardless of the Schottky barrier role when an applied voltage has already reached a few tens of volts. First, we note that BNNTs are noncentrosymmetric and are naturally polar. Therefore, they have been suggested to possess piezoelectricity.[9,10] Schematic illustration of the model is shown in Figure 4b. In this measurement setup, one circuit end is grounded. Because BNNTs are bent by approaching two electrodes, a compression strain should dominate the overall elastic deformation. This induces the

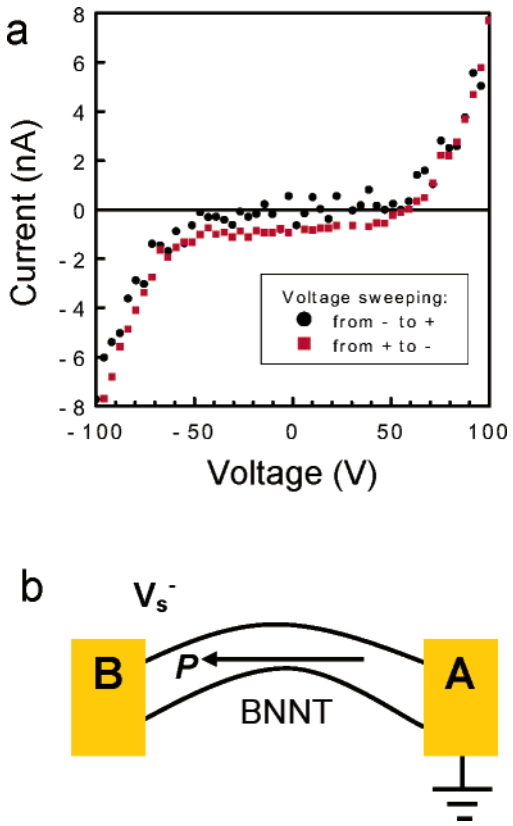

Figure 4. (a) Representative $I-V$ hysteresis loop obtained on a deformed BNNT when a bias voltage is sweeping from negative to positive and from positive to negative values. (b) Schematic model of a transport circuit which includes a piezoelectric BNNT. An arrowed label *P* shows the direction of polarization.

spontaneous polarization along a BNNT. The grounded electrode **A** has a potential of nearly zero, and another electrode **B** has a negative potential, thus a polarization field from **A** to **B** is formed. When a negative voltage is applied along a BNNT, the directions of the applied field and polarization field would coincide; the carrier transport becomes smooth. When a positive voltage is applied, the directions of the applied field and polarization field become opposite; the transport is now obstructed so that a current in the negative voltage region is usually larger than that in the positive voltage region. If the voltage sweeping pathway is reversed, from positive to negative, and an applied voltage reaches ~60 V the applied field and polarization field effects exactly counteract and the current becomes zero. Hereafter, the polarization field dominates the carrier transport at a low bias.

Other possible factors responsible for the observed $I-V$ curve hysteresis, e.g., heating effect, etc., were also taken into account in the present work. It is worth noting that when the direction of voltage sweeping is reversed (from + to −), the current becomes negative even at the positive voltage region. If the hysteresis is due to a heating effect, the current should be positive at the positive voltage region. Thus the heating effect can be excluded. We have performed this experiment on many BNNT samples. The similar $I-V$ hysteresis-like curves were obtained. It is also noted that the hysteresis has not resulted from the signal noise. To sum up, the phenomenon is obvious enough for the BNNTs in which the piezoelectricity is not very strong and is hardly detected experimentally. Therefore, our data suggest that the $I-V$ hysteresis-like curves result from the piezoelectric effect rather than other effects.

It is finally emphasized here that the locally deformed BNNTs are assumed to be highly useful in smart nanodevice applications. In fact, because the severity of BNNT flattening changes along the nanotube, the bent BNNT itself becomes a kind of a heterostructure; it may directly act as a local optical detector and sensor in advanced miniaturized nanodevices.

In summary, we performed in situ manipulation and electrical transport measurements on individual multiwalled BNNTs inside a high-resolution transmission electron microscope. Remarkably, the nanotube electrical transport properties were found to be smoothly tuned from insulating to semiconducting through a bending deformation. Importantly, such unique transition was reversible. The BNNT semiconductor parameters were retrieved from the experimental $I-V$ data. Resultantly, it was confirmed that the unmatched transition in the BNNT electrical performance had been governed by deformation. $I-V$ hysteresis existed in bent BNNTs under the change in a bias voltage sweeping polarity, which could be a sign of BNNT piezoelectricity. Keeping in mind that BNNTs possess excellent mechanical properties and are ultralightweight materials, the discovered deformation-driven tuning of BNNT electrical appearance and piezoelectricity may have many interesting prospective applications in the nanoscale sensors, actuators, and advanced NEMS devices with integrated electronic/optical functions.

Acknowledgment. We thank Drs. Y. Uemura and O. Lourie for the continuous technical support over the course of this work.

Supporting Information Available: Experimental details describing preparation and performance of a multiwalled BNNT-based field-effect transistor, additional $I-V$ curves verifying a deformation-driven electrical transport of individual BNNTs when Pt or Au−W electrodes were used instead of Au electrodes during in situ TEM probing, electron diffraction pattern, and electron loss energy spectrum (EELS) of analyzed BNNTs, and changes of the EELS spectra fine structure under BNNT bending. This material is available free of charge via the Internet at http://pubs.acs.org.

References

(1) Rubio, A.; Corkill, J. L.; Cohen, M. L. *Phys. Rev. B* **1994**, *49*, 5081.
(2) Blase, X.; Rubio, A.; Louie, S. G.; Cohen, M. L. *Europhys. Lett.* **1994**, *28*, 335.
(3) Cumings, J.; Zettl, A. *Solid State Commun.* **2004**, *129*, 661.
(4) Kim, Y. H.; Chang, K. J.; Louie, S. G. *Phys. Rev. B* **2001**, *63*, 205408.
(5) Hernández, E.; Goze, C.; Bernier, P.; Rubio, A. *Phys. Rev. Lett.* **1998**, *80*, 4502.
(6) Suryavanshi, A. P.; Yu, M.-F.; Wen, J.; Tang, C.; Bando, Y. *Appl. Phys. Lett.* **2004**, *84*, 2527.
(7) Chopra, N. G.; Zettl, A. *Solid State Commun.* **1998**, *105*, 297.
(8) Bettinger, H. F.; Dumitrica, T.; Scuseria, G. E.; Yakobson, B. I. *Phys. Rev. B* **2002**, *65*, 041406.
(9) Michalski, P. J.; Sai, N.; Mele, E. J. *Phys. Rev. Lett.* **2005**, *95*, 116803.
(10) Mele, E. J.; Kral, P. *Phys. Rev. Lett.* **2002**, *88*, 056803.
(11) Nakhmanson, S. M.; Calzolari, A.; Meunier, V.; Bernholc, J.; Nardelli, M. B. *Phys. Rev. B* **2003**, *67*, 235406.

(12) Svensson, K.; Jompol, Y.; Olin, H.; Olsson, E. *Rev. Sci. Instrum.* **2003**, *74*, 4945.
(13) http://www.nanofactory.com.
(14) Tang, C.; Bando, Y.; Sato, T.; Kurashima, K. *Chem. Commun.* **2002**, *12*, 1290.
(15) Golberg, D.; Mitome, M.; Kurashima, K.; Zhi, C. Y.; Tang, C. C.; Bando, Y.; Lourie, O. *Appl. Phys. Lett.* **2006**, *88*, 123101.
(16) Golberg, D.; Bai, X. D.; Mitome, M.; Tang, C.; Zhi, C.Y.; Bando, Y. *Acta Mater*. **2007**, *55*, 1293.
(17) Poncharal, P.; Wang, Z. L.; Ugarte, D.; de Heer, W. A. *Science* **1999**, *283*, 1513.
(18) Appenzeller, J.; Radosavljevic, M.; Knoch, J.; Avouris, Ph. *Phys. Rev. Lett.* **2004**, *92*, 048301.
(19) Padovani, F. A.; Stratton, R. *Solid-State Electron.* **1966**, *9*, 695.
(20) Zhang, Z. Y.; Jin, C. H.; Liang, X. L.; Chen, Q.; Peng, L.-M. *Appl. Phys. Lett.* **2006**, *88*, 073102.
(21) Han, X. D.; Zhang, Y. F.; Zheng, K.; Zhang, X. N.; Zhang, Z.; Hao, Y. J.; Guo, X. Y.; Yuan, J.; Wang, Z. L. *Nano Lett.* **2007**, http://dx.doi.org/10.1021/nl0627689.

NL062540L